NOTICE: This is the author’s version of a work that was accepted for publication in Advances in Space Research. Changes resulting from the publishing process, such as peer review, editing, corrections, structural formatting, and other quality control mechanisms may not be reflected in this document. Changes may have been made to this work since it was submitted for publication. A definitive version was subsequently published in Advances in Space Research, Vol. 54, Issue 5. (2014). doi: 10.1016/j.asr.2013.08.030

# Instantaneous COMPASS-GPS Attitude Determination: A Robustness Analysis

Nandakumaran Nadarajah[1,*], Peter J. G. Teunissen[1,2], Noor Raziq[1]

**Abstract**

The advent of modernized and new global navigation satellite systems (GNSS) has enhanced the availability of satellite based positioning, navigation, and timing (PNT) solutions. Specifically, it increases redundancy and yields operational back-up or independence in case of failure or unavailability of one system. Among existing GNSS, the Chinese COMPASS navigation satellite system (CNSS) is being developed and will consist of geostationary (GEO) satellites, inclined geosynchronous orbit (IGSO) satellites, and medium-Earth-orbit (MEO) satellites. In this contribution, a COMPASS-GPS robustness analysis is carried out for instantaneous, unaided attitude determination.

Precise attitude determination using multiple GNSS antennas mounted on a platform relies on the successful resolution of the integer carrier phase ambiguities. The constrained Least-squares AMBiguity Decorrelation Adjustment (C-LAMBDA) method has been developed for the quadratically constrained GNSS compass model that incorporates the known baseline length. In this contribution the method is used to analyse the attitude determination performance when using the GPS and COMPASS systems. The attitude determination performance is evaluated using GPS/COMPASS data sets from a real data campaign in Australia spanning several days. The study includes the performance analyses of both stand-alone and mixed constellation (GPS/COMPASS) attitude estimation under various satellite deprived environments. We demonstrate and quantify the improved availability, reliability, and accuracy of attitude determination using the combined constellation.

*Keywords:* GNSS, GPS, COMPASS, attitude determination, constrained integer least-squares, C-LAMBDA, carrier phase ambiguity resolution

## 1. Introduction

The advent of modernized and new global navigation satellite systems (GNSS) has enhanced the availability of satellite based positioning, navigation, and timing (PNT) solutions. Specifically, it increases redundancy and yields operational back-up or independence in case of failure or unavailability of one system. Among existing GNSS, the Chinese COMPASS navigation satellite system (CNSS) is being developed and will consist of geostationary (GEO) satellites, inclined geosynchronous orbit (IGSO) satellites, and medium-Earth-orbit (MEO)



*Corresponding author

*Email addresses:* N.Nadarajah@Curtin.edu.au (Nandakumaran Nadarajah), P.Teunissen@Curtin.edu.au (Peter J. G. Teunissen), Noor.Raziq@Curtin.edu.au (Noor Raziq)

[1]GNSS Research Centre, Department of Spatial Sciences, Curtin University, GPO Box U1987, Perth, WA 6845, Australia

[2]Delft Institute of Earth Observation and Space Systems (DEOS), Delft University of Technology, PO Box 5058, 2600 GB Delft, The Netherlands

satellites (CSNO, 2011; Cao et al., 2008). Presently, the COMPASS/BeiDou-2 system consists of four fully operational GEO and five IGSO satellites transmitting navigation signals in quadrature phase-shift keying (QPSK) modulation on a total of three frequency bands (B1, B2, B3). Analyses of COMPASS based PNT solutions have been reported in various studies. Apart from simulation based studies in Grelier et al. (2007); Chen et al. (2009); Yang et al. (2011); Zhang et al. (2011), analyses with real data have been reported in Montenbruck et al. (2012b,a); Shi et al. (2012); Steigenberger et al. (2012a). Measurement quality and relative positioning analyses with real data collected using Chinese GNSS receivers (UB240-CORS) have been reported in Shi et al. (2012). Montenbruck et al. (2012b) discussed initial assessment of real data collected using non-Chinese GNSS receivers and with post-processed orbit and clock products (Steigenberger et al., 2012b) independent of the control segment. The same products have been used to analyze precise point positioning in Steigenberger et al. (2012a) and triple-frequency relative positioning in Montenbruck et al. (2012a).

In this contribution, a robustness analysis of attitude determination using the standalone COMPASS system, and the combined GPS and COMPASS systems is carried out. Multiple GNSS receivers/antennas rigidly mounted on a platform can be used to determine platform attitude (orientation) (see, for example, Cohen, 1992; Lu, 1995; Crassidis and Markley, 1997; Li et al., 2004; Lin et al., 2004; Madsen and Lightsey, 2004; Psiaki, 2006). GNSS-based attitude determination offers several advantages including that it is not affected by drift, is lower in cost and requires less maintenance than traditional methods. Precise attitude determination, however, relies on successful resolution of the integer carrier phase ambiguities. The Least squares AMBiguity Decorrelation Adjustment (LAMBDA) method (Teunissen, 1995) is currently the standard method for solving unconstrained and linearly constrained GNSS ambiguity resolution problems (see, for example, Boon and Ambrosius, 1997; Cox, 1999; Ji et al., 2007; Huang et al., 2009; Kroes et al., 2005; Jin et al., 2010, 2005; Park, 2002). For such models, the method is known to be numerically efficient and optimal in the sense that it provides integer ambiguity solutions with the highest possible success-rate (Teunissen, 1999; Teunissen et al., 1997; Verhagen and Teunissen, 2006a). To exploit the known baseline length, we make use of the constrained (C-)LAMBDA method (Park and Teunissen, 2003; Teunissen, 2006; Buist, 2007; Park and Teunissen, 2009; Giorgi et al., 2008; Giorgi and Buist, 2008; Teunissen, 2010; Giorgi et al., 2010; Teunissen et al., 2011). Due to the rigorous inclusion of the known baseline length, significantly higher success rates will be demonstrated.

Our analyses are carried out using data sets from real data campaign spanning several days. Based on this static data, we analysed the performance of the C-LAMBDA method comparing the standard LAMBDA method. Kinematic analyses of C-LAMBDA method can be found in (Giorgi et al., 2012a,b). Since satellite navigation data of the COMPASS system is not publicly available at the time of writing, we use off-line navigation from post-processed orbit and clock information derived from an experimental regional network of monitoring stations in Australia, Asia and Russia (Steigenberger et al., 2012a,b). We evaluate the epoch-by-epoch, single- and multi-frequency integer ambiguity resolution performance of the C-LAMBDA method under various satellite deprived environments such as the presence of satellite blockages due to urban canyon. Our analyses are the first reported results of GNSS attitude determination using real data from the COMPASS/BeiDou2 system and demonstrate the increased availability of GNSS-based attitude solution by the inclusion of COMPASS/BeiDou-2 system.

This contribution is organized as follows. Section 2 presents our attitude determination method using multi-constellation GNSS data. First, it describes the phase and code observation equations for short-baseline GPS+COMPASS positioning. Then, it formulates the quadratically constrained GPS+COMPASS model, followed by a description of the C-LAMBDA method for attitude determination. Section 3 presents the results of the performance evaluation for combined constellation ambiguity resolution and attitude determination under various satellite deprived environments, while Section 4 draws conclusions of this contribution.

## 2. The GNSS-Based Attitude Determination

In this section we present our attitude determination method using the combined GPS-COMPASS system. First we describe the functional and stochastic model for the combined observations and then we present the steps for solving the baseline constrained, mixed-integer attitude model.

### *2.1. GPS/COMPASS Observations*

Since the GPS and COMPASS system do not have frequencies in common, we consider system-specific double differencing (Verhagen and Joosten, 2003). Let us consider two GPS/COMPASS receivers $r$ and 1 forming a short baseline and tracking $m_G+1$ GPS satellites and $m_C+1$ COMPASS satellites. The double difference (DD) pseudo-range and carrier-phase observations at frequency $j$ for satellite pairs 1-$s$ of GNSS system $\Xi$ (G for GPS and C for COMPASS), denoted as $p_{1r}^{1s,\Xi}$ and $\phi_{1r}^{1s,\Xi}$ respectively, are given as (Teunissen and Kleusberg, 1998)

$$\mathrm{E}\left(p_{1r,j}^{1s,\Xi}\right) = \rho_{1r}^{1s,\Xi}, \qquad s = 2,\ \ldots,\ (m_\Xi + 1) \tag{1}$$

$$\mathrm{E}\left(\phi_{1r,j}^{1s,\Xi}\right) = \rho_{1r}^{1s,\Xi} + \lambda_j^{;\Xi} N_{1r,j}^{1s,\Xi}, \qquad s = 2,\ \ldots,\ (m_\Xi + 1) \tag{2}$$

where $\mathrm{E}(\cdot)$ denotes the expectation operator, $\rho_{1r}^{1s,\Xi}$ is the DD topocentric distance, $\lambda_j^{;\Xi}$ is the wave length, and $N_{1r,j}^{1s,\Xi}$ is the time-invariant *integer* DD carrier-phase ambiguity.

The linearized DD observation equations corresponding to (1) and (2), read

$$\mathrm{E}\left(\Delta p_{1r,j}^{1s,\Xi}\right) = g_1^{1s,\Xi^T} b, \qquad s = 2,\ \ldots,\ (m_\Xi + 1) \tag{3}$$

$$\mathrm{E}\left(\Delta\phi_{1r,j}^{1s,\Xi}\right) = g_1^{1s,\Xi^T} b + \lambda_j^{;\Xi} N_{1r,j}^{1s,\Xi}, \qquad s = 2,\ \ldots,\ (m_\Xi + 1) \tag{4}$$

where $\Delta p_{1r,j}^{1s,\Xi}$ and $\Delta\phi_{1r,j}^{1s,\Xi}$ are the observed-minus-computed code and phase observations, $b$ is the baseline vector containing relative position components, and $g_1^{1s,\Xi}$ is the geometry vector given as $g_1^{1s,\Xi} = e_1^{1,\Xi} - e_1^{s,\Xi}$ with $e_r^{s,\Xi}$ the unit line-of-sight vector between receiver-satellite pair $r-s$. The vector form of the DD observation equation for the $j$th frequency read

$$\mathrm{E}(y_{p;j}^{,\Xi}) = G_1^{,\Xi} b \tag{5}$$

$$\mathrm{E}(y_{\phi;j}^{,\Xi}) = G_1^{,\Xi} b + \lambda_j^{,\Xi} z_{r,j}^{,\Xi} \tag{6}$$

with $y_{p;j}^{,\Xi} = \left[\Delta p_{1r,j}^{12,\Xi} \ \ldots \ \Delta p_{1r,j}^{1(m_\Xi+1),\Xi}\right]^T$, $y_{\phi;j}^{,\Xi} = \left[\Delta \phi_{1r,j}^{12,\Xi} \ \ldots \ \Delta \phi_{1r,j}^{1(m_\Xi+1),\Xi}\right]^T$, $G_1^{,\Xi} = \left[g_1^{12,\Xi} \ \ldots \ g_1^{1(m_\Xi+1),\Xi}\right]^T$, $z_{r,j}^{,\Xi} = \left[N_{1r,j}^{12,\Xi} \ \ldots \ N_{1r,j}^{1(m_\Xi+1),\Xi}\right]^T$.

For stochastic modeling, we assume elevation dependent noise characteristics (Euler and Goad, 1991). That is, the standard deviation of the undifferenced observable $\varsigma$ can be written as

$$\sigma_\varsigma(\epsilon) = \sigma_{\varsigma 0}\left(1 + a_{\varsigma 0}\exp\left(\frac{-\epsilon}{\epsilon_{\varsigma 0}}\right)\right) \tag{7}$$

where $\epsilon$ is the elevation angle of the corresponding satellite, and $\sigma_{\varsigma 0}$, $a_{\varsigma 0}$, and $\epsilon_{\varsigma 0}$ are the elevation dependent model parameters. We further assume that the receivers have similar characteristics and that the observation noise standard deviations can be decomposed as follows:

$$\begin{aligned} \sigma_{\phi_{r,j}^{s,\Xi}} &= \sigma_r \sigma_{\phi_0} \sigma_{,j} \sigma^{,\Xi} \nu^{s,\Xi} \\ \sigma_{p_{r,j}^{s,\Xi}} &= \sigma_r \sigma_{p_0} \sigma_{,j} \sigma^{,\Xi} \nu^{s,\Xi} \\ \nu^{s,\Xi} &= \left(1 + a_0 \exp\left(\frac{-\epsilon^{s,\Xi}}{\epsilon_0}\right)\right) \end{aligned} \tag{8}$$

where $\sigma_r$, $\sigma^{,\Xi}$, and $\sigma_{,j}$ are the receiver, the system, and the frequency dependent weightings, respectively, and $\sigma_{\phi_0}$ and $\sigma_{p_0}$ are observation dependent weightings.

### *2.2. The GPS/COMPASS Attitude Model*

When combining the single-epoch, multi-frequency linearized DD GNSS code and phase observation equations of (5) and (6), we obtain the mixed integer model of observation equations:

$$\mathrm{E}(y) = Az + Gb \qquad z \in \mathbb{Z}^{fm}, b \in \mathbb{R}^3 \tag{9}$$

where $m = m_G + m_C$, $y = [y_\phi^T \ y_p^T]^T$ is the $2fm \times 1$ vector of linearized (observed-minus-computed) DD observations with $y_\phi = [y_\phi^{,G\,T} \ y_\phi^{,C\,T}]^T$, $y_\phi^{,\Xi} = [y_{\phi;1}^{,\Xi\ T}, \ldots, y_{\phi;f}^{,\Xi\ T}]^T$, $y_p = [y_p^{,G\,T} \ y_p^{,C\,T}]^T$, and $y_p^{,\Xi} = [y_{p;1}^{,\Xi\ T}, \ldots, y_{p;f}^{,\Xi\ T}]^T$, $z = [z^{,G\,T}, z^{,C\,T}]^T$ is the $fm \times 1$ vector of unknown DD integer ambiguities with $z^{,\Xi} = [z_{,1}^{,\Xi T}, \ldots, z_{,f}^{,\Xi T}]^T$, $b$ is $3 \times 1$ vector unknown baseline parameters, $G = e_2 \otimes [(e_f \otimes G_1^{,G})^T, \ (e_f \otimes G_1^{,C})^T]^T$ is the $2fm \times 3$ geometry matrix with $e_n$ the $n \times 1$ vector of 1's, $A = [L^T \ 0^T]^T$ is the $2fm \times fm$ design matrix with $fm \times fm$ matrix $L =$

blockdiag$(\Lambda^{G} \otimes I_{m_G}, \Lambda^{C} \otimes I_{m_C})$ and $\Lambda^{\Xi} = \mathrm{diag}(\lambda_1^{,\Xi}, \ldots, \lambda_f^{,\Xi})$ the diagonal wavelength matrix, with $\otimes$ denoting the Kronecker product (Harville, 1997; Magnus and Neudecker, 1995).

To construct the stochastic model for the observations in (9), consider the undifferenced observations reading

$$\zeta = [\zeta_1^T \ \zeta_2^T]^T \tag{10}$$

where $\zeta_r = [\phi_r^T \ p_r^T]^T$, $\phi_r = [\phi_r^{,G\,T} \ \phi_r^{,C\,T}]^T$, $\phi_r^{,\Xi} = [\phi_{r,1}^{,\Xi\ T} \ \ldots \ \phi_{r,f}^{,\Xi\ T}]^T$, $\phi_{r,j}^{,\Xi} = [\phi_{r,j}^{1,\Xi} \ \ldots \phi_{r,j}^{m_\Xi+1,\Xi}]^T$, $p_r = [p_r^{,G\,T} \ p_r^{,C\,T}]^T$, $p_r^{,\Xi} = [p_{r,1}^{,\Xi\ T} \ \ldots \ p_{r,f}^{,\Xi\ T}]^T$, $p_{r,j}^{,\Xi} = [p_{r,j}^{1,\Xi} \ \ldots p_{r,j}^{m_\Xi+1,\Xi}]^T$, and $p_{r,j}^{s,\Xi}$ and $\phi_{r,j}^{s,\Xi}$ are the undifferenced code and phase observations for $r-s$ receiver-satellite pair at $j$th frequency. Using the noise characteristics of (8) and assuming that the observables are normally distributed and mutually uncorrelated, the dispersion matrix of the observation vector $\zeta$ can be written as

$$\mathrm{D}(\zeta) \quad = \quad Q_r \otimes Q_t \otimes \mathrm{blockdiag}(Q_f \otimes Q_G, Q_f \otimes Q_C) \tag{11}$$

where $\mathrm{D}(\cdot)$ denotes the dispersion operator, $Q_r = \mathrm{diag}[\sigma_1^2 \ \sigma_2^2]$, $Q_t = \mathrm{diag}[\sigma_{\phi_0}^2 \ \sigma_{p_0}^2]$, $Q_f = \mathrm{diag}[\sigma_{,1}^2 \ \ldots \ \sigma_{,f}^2]$, $Q_G = \sigma^{,G^2}\mathrm{diag}[\nu^{1,G^2} \ \ldots \ \nu^{m_G+1,G^2}]$, and $Q_C = \sigma_{,C}{}^2\mathrm{diag}[\nu^{1,C^2} \ \ldots \ \nu^{m_C+1,C^2}]$ are the co-factor matrices. The dispersion matrix of the DD observations is then given as

$$\mathrm{D}(y) = \mathrm{D}(\mathcal{D}^T\zeta) = Q_{yy} \tag{12}$$

with the DD operator $\mathcal{D}^T = D_1^T \otimes I_2 \otimes \mathrm{blockdiag}\left(I_f \otimes D_{m_G}^T, \ I_f \otimes D_{m_C}^T\right)$, in which $D_n^T = [-e_n, \ I_n]$ is the differencing matrix.

The DD observation equations of (9) form, together with the dispersion matrix of (12), a *mixed-integer* Gauss-Markov model with unknown integer vector $z \in \mathbb{Z}^{fm}$ and unknown baseline vector $b \in \mathbb{R}^3$. This model can be strengthened with the known baseline length. With the inclusion of the baseline length constraint, we obtain the GNSS compass model (Teunissen, 2006, 2010)

$$\mathrm{E}(y) \quad = \quad Az + Gb \qquad \|b\| = l, z \in \mathbb{Z}^{fm}, b \in \mathbb{R}^3 \tag{13}$$

$$\mathrm{D}(y) \quad = \quad Q_{yy} \tag{14}$$

where $l$ is the known baseline length and $\|\cdot\|$ denotes the unweighted norm. Hence, the baseline is thus now constrained to lie on a sphere with radius $l$ ($\mathbb{S}_l = \left\{b \in \mathbb{R}^3 | \ \|b\| = l\right\}$). Our objective is to solve for $b$ in a least-squares sense, thereby taking the integer constraints on $z$ and the quadratic constraint on vector $b$ into account. Hence, the least-squares minimization problem that will be solved reads

$$\min_{z \in \mathbb{Z}^{fm}, b \in \mathbb{S}_l} \|y - Az - Gb\|_{Q_{yy}}^2 \tag{15}$$

with $||\cdot||_Q^2 = (\cdot)^T Q^{-1}(\cdot)$. It is a quadratically constrained (mixed) integer least-squares (QC-ILS) problem (Park and Teunissen, 2003), for which no closed-form solution is available. In the following sections, we describe the method for solving (15).

*2.3. The Ambiguity Resolved Attitude*

We now describe the steps for computing the integer ambiguity resolved attitude angles.

*2.3.1. The real-valued float solution:*

The float solution is defined as the solution of (15) without the constraints. When we ignore the integer constraints on $z$ and the quadratic constraint on $b$, the float solutions $\hat{z}$ and $\hat{b}$, and their variance-covariance matrices are obtained as follows:

$$\begin{bmatrix} Q_{\hat{z}\hat{z}} & Q_{\hat{z}\hat{b}} \\ Q_{\hat{b}\hat{z}} & Q_{\hat{b}\hat{b}} \end{bmatrix}^{-1} \cdot \begin{bmatrix} \hat{z} \\ \hat{b} \end{bmatrix} = \begin{bmatrix} A^T \\ G^T \end{bmatrix} Q_{yy}^{-1} y \tag{16}$$

with

$$\begin{bmatrix} Q_{\hat{z}\hat{z}} & Q_{\hat{z}\hat{b}} \\ Q_{\hat{b}\hat{z}} & Q_{\hat{b}\hat{b}} \end{bmatrix} = \left( \begin{bmatrix} A^T \\ G^T \end{bmatrix} Q_{yy}^{-1} \begin{bmatrix} A & G \end{bmatrix} \right)^{-1} \tag{17}$$

The $z$-constrained solution of $b$ and its variance-covariance matrix can be obtained from the float solution as follows

$$\begin{aligned} \hat{b}(z) &= \hat{b} - Q_{\hat{b}\hat{z}} Q_{\hat{z}\hat{z}}^{-1} (\hat{z} - z) && (18) \\ Q_{\hat{b}(z)\hat{b}(z)} &= Q_{\hat{b}\hat{b}} - Q_{\hat{b}\hat{z}} Q_{\hat{z}\hat{z}}^{-1} Q_{\hat{z}\hat{b}} \\ &= \left( G^T Q_{yy}^{-1} G \right)^{-1} && (19) \end{aligned}$$

Using the above estimators, the original problem in (15) can be decomposed as

$$\begin{aligned} &\min_{z \in \mathbb{Z}^{fm}, b \in \mathbb{S}_l} \|y - Az - Gb\|_{Q_{yy}}^2 \\ = \;& \|\hat{e}\|_{Q_{yy}}^2 + \min_{z \in \mathbb{Z}^{fm}} \left( \|\hat{z} - z\|_{Q_{\hat{z}\hat{z}}}^2 + \min_{b \in \mathbb{S}_l} \left\| \hat{b}(z) - b \right\|_{Q_{\hat{b}(z)\hat{b}(z)}}^2 \right) \end{aligned} \tag{20}$$

with $\hat{e} = y - A\hat{z} - G\hat{b}$ being the vector of least-squares residuals. Note that the first term on the right hand side of (20) does not depend on the unknown parameters $z$ and $b$ and is therefore constant.

*2.3.2. The integer ambiguity resolution:*

Based on the orthogonal decomposition (20), the quadratic constrained integer minimization can be formulated as:

$$\check{z} = \arg \min_{z \in \mathbb{Z}^{fm}} C(z) \tag{21}$$

with ambiguity objective function

$$C(z) = \|\hat{z} - z\|_{Q_{\hat{z}\hat{z}}}^2 + \left\| \hat{b}(z) - \check{b}(z) \right\|_{Q_{\hat{b}(z)\hat{b}(z)}}^2 \tag{22}$$

where

$$\check{b}(z) \quad = \quad \arg\min_{b \in \mathbb{S}_l} \left\| \hat{b}(z) - b \right\|^2_{Q_{\hat{b}(z)\hat{b}(z)}} \tag{23}$$

The cost function $C(z)$ is the sum of two coupled terms: the first weighs the distance from the float ambiguity vector $\hat{z}$ to the nearest integer vector $z$ in the metric of $Q_{\hat{z}\hat{z}}$, while the second weighs the distance from the conditional float solution $\hat{b}(z)$ to the nearest point on the sphere $\mathbb{S}_l$ in the metric of $Q_{\hat{b}(z)\hat{b}(z)}$.

Unlike with the standard LAMBDA method (Teunissen, 1995), the search space of the above minimization problem is non-ellipsoidal due to the presence of the second term in the ambiguity objective function. Moreover, its solution requires the computation of a nonlinear constrained least-squares problem (23) for every integer vector in the search space. In the C-LAMBDA method, this problem is mitigated through the use of easy-to-evaluate bounding functions (Teunissen, 2010). Using these bounding functions, two strategies, namely the *Expansion* and the *Search and Shrink* strategies, were developed, see e.g. Park and Teunissen (2003); Giorgi et al. (2008). These techniques avoid the computation of (23) for every integer vector in the search space, and compute the integer minimizer $\check{z}$ in an efficient manner.

#### *2.3.3. The ambiguity resolved attitude:*

Finally, we obtain the ambiguity resolved attitude solution by substituting $\check{z}$ into (18), thus giving $\hat{b}(\check{z})$. For a single baseline, $b$ is related to the Euler-angles $\xi = [\phi\ \theta]^T$, with $\phi$ the heading and $\theta$ the elevation, as $b(\xi) = lu(\xi)$, where $u(\xi) = [c_\theta c_\phi,\ c_\theta s_\phi,\ -s_\theta]^T$ with $s_\alpha = \sin(\alpha)$ and $c_\alpha = \cos(\alpha)$. Hence, the sought-for attitude angles $\xi(\check{z})$ are then obtained by solving the following nonlinear least squares problem:

$$\begin{aligned} \mathrm{E}\left(\hat{b}(\check{z})\right) &= lu(\xi) \\ \mathrm{D}\left(\hat{b}(\check{z})\right) &= Q_{\hat{b}(z)\hat{b}(z)} \end{aligned} \tag{24}$$

Using a first order approximation, the formal variance-covariance matrix of the ambiguity resolved, least-squares estimated heading and elevation angles is given by

$$Q_{\hat{\xi}\hat{\xi}} \approx \frac{1}{l^2}\left(J_{u,\xi}(\hat{\xi})^T Q^{-1}_{\hat{b}(z)\hat{b}(z)} J_{u,\xi}(\hat{\xi})\right)^{-1} \tag{25}$$

with Jacobian matrix

$$J_{u,\xi}(\xi) \quad = \quad \begin{bmatrix} -s_\phi c_\theta & -c_\phi s_\theta \\ c_\phi c_\theta & -s_\phi s_\theta \\ 0 & -c_\theta \end{bmatrix} \tag{26}$$

As the results in the next section show, this first order approximation works well. This is due to the fact that the ambiguity resolved solution is driven by the high precision of the carrier phase observables.


(a) Antenna setup

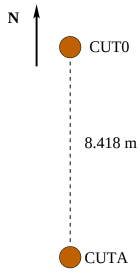


(b) Antenna geometry

Figure 1: Curtin GNSS antennas used for the real data campaign

| System | Frequency | Code | | | Phase | | |
|---|---|---|---|---|---|---|---|
| | | $\sigma_{p_0}$ [cm] | $a_{p_0}$ | $\epsilon_{p_0}$ [deg] | $\sigma_{\phi_0}$ [mm] | $a_{\phi_0}$ | $\epsilon_{\phi_0}$ [deg] |
| GPS | L1 | 15 | 5 | 20 | 1 | 5 | 20 |
| | L2 | 20 | 2 | 15 | 2 | 6 | 15 |
| COMPASS | B1 | 20 | 5 | 15 | 1 | 5 | 15 |
| | B2 | 20 | 5 | 15 | 2 | 5 | 15 |
| | B3 | 20 | 5 | 15 | 3 | 5 | 15 |

Table 1: Elevation dependent stochastic model parameters (7) for Curtin GNSS stations used in the real data campaigns

## 3. Performance of GPS/COMPASS Attitude Determination

In this section the performance analyses of GPS/COMPASS attitude determination are presented. The data was collected from two TRM59800.00-SCIS antennas mounted on the roof of the Bentley campus building 402 of Curtin University in Perth, Australia. As shown in Figure 1(a), the antennas are free of obstacles and form a short baseline ($B_0$ = 8.418 m, Figure 1(b)). These antennas are connected to two TRIMBLE NETR9 GNSS receivers continuously tracking all available GNSS satellites. We processed GPS/COMPASS data for 23 days (from March 20, 2012 to April 11, 2012) with a sampling interval of 30 sec. Since satellite navigation data is not yet publicly available for the COMPASS system, we used off-line navigation from post-processed orbit and clock information derived from an experimental regional network of monitoring stations in Australia, Asia and Russia (Steigenberger et al., 2012a,b). Figure 2 shows the GPS/COMPASS satellite visibility on March 21, 2012 (the skyplots, the number of satellites, and the PDOP values) demonstrating improved satellite visibility of the combined system. The stochastic model parameters of the elevation dependent model (7) for the receivers are reported in Table 1.

We considered two performance measures for our analyses; the first one is the empirical instantaneous ambiguity success fraction (relative frequency), which

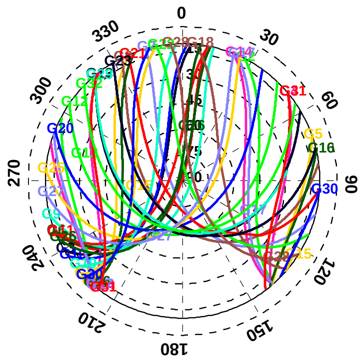


(a) Skyplot (GPS)

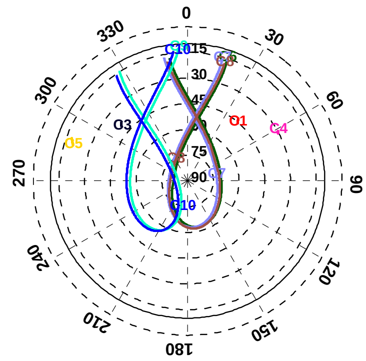


(b) Skyplot (COMPASS)

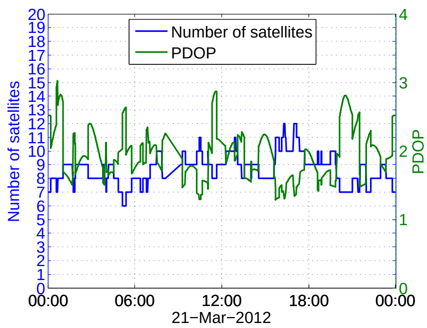


(c) Number of satellites and PDOP (GPS)

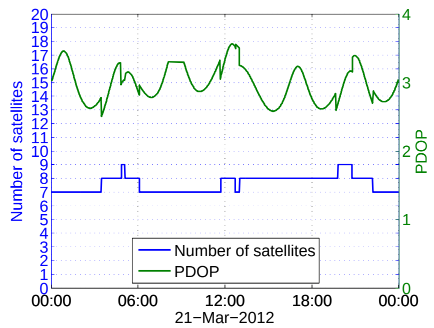


(d) Number of satellites and PDOP (COMPASS)

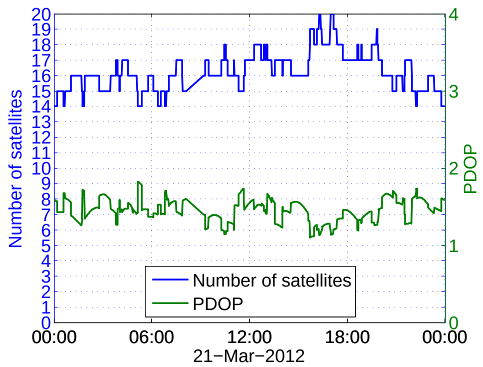


(e) Number of satellites and PDOP (Combined)

Figure 2: Satellite visibility of GPS and COMPASS constellations on March 21, 2012 for 10° elevation cut-off

is defined as

$$\text{success fraction} = \frac{\text{number of correctly fixed epochs}}{\text{total number of epochs}} \quad (27)$$

The second one is the angular estimation accuracy, which is given by the formal and empirical standard deviations of attitude angular estimates.

In the following, our robustness analysis is carried out for single- (L1 and/or B1), dual- (L1 and L2 and/or B1 and B2), and triple- (L1, L2, and L5 and/or B1, B2, and B3) frequency attitude determination under three satellite deprived environments, namely, open-pit (Section 3.1), satellite outage (Section 3.2), and urban canyon (Section 3.3). Note that, for triple-frequency processing, we only considered standalone COMPASS processing (B1, B2, and B3) as the third frequency (L5) of GPS system is only available from PRN 1 and 25, and they have not been co-visible during the period considered.

### *3.1. Open-pit*

In this section, the impact of an open-pit environment on attitude estimation is analyzed. As shown in Figure 3 the platform is assumed to be at the center of an open-pit base. The performance at any other location can be inferred from the performance at the center with average elevation masking angle at that location. Table 2 reports the ambiguity resolution success fractions for single-, dual-, and triple-frequency processing, highlighting (in bold text) the benefits of using a combined system, which clearly improves the availability of attitude solutions.

The benefits of using multi-frequency data are also highlighted with emphasized text. Note that, for large elevation masking angles, a fraction of epochs (given in brackets) were processed due to a lack of sufficient visible satellites for positioning (requires at least four satellites). The *single-frequency* C-LAMBDA processing of a combined system enables the availability of instantaneous attitude solutions for an open-pit with up to 30 deg elevation masking, while a standalone system with dual frequency processing can provide instantaneous attitude solution for an open-pit with only up to 20 deg elevation masking. The angular scatter plots for $10^\circ$ elevation masking are given in Figure 4 depicting improved performance of the combined system. Due to the baseline length and the relatively poor precision of the second and the third frequency observables (Table 1), multi-frequency processing does not really improve the performance angular accuracy over the single-frequency processing. Therfore the angular accuracies (standard deviations) of only the single frequency processing are reported in Table 3 (Results for high elevation maskings are omitted due to a lack of sufficient data). As shown, increasing elevation masking degrades both ambiguity resolution and the angular accuracy.

### *3.2. Satellite Outage*

This satellite deprived environment is simulated by arbitrarily removing a number of visible GPS or COMPASS satellites. Table 4 reports the LAMBDA

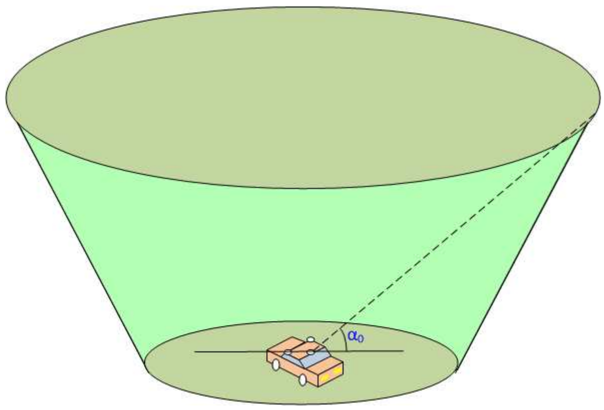


Figure 3: Simulated circular open-pit; the elevation masking angle $\alpha_o$ defines the blockage. The platform is assumed to be at the center of open-pit base

| Number of Frequency | Elevation Cut-off [deg] | GPS only | | COMPASS only | | GPS + COMPASS | |
|---|---|---|---|---|---|---|---|
| | | LAMBDA | C-LAMBDA | LAMBDA | C-LAMBDA | LAMBDA | C-LAMBDA |
| 1 | 10 | 0.83 | 0.99 | 0.50 | 0.96 | **1.00** | **1.00** |
| | 20 | 0.49 | 0.93 | 0.36 | 0.93 | **1.00** | **1.00** |
| | 30 | 0.15 | 0.70 (0.93) | 0.19 | 0.72 (0.96) | 0.95 | **1.00** |
| | 40 | 0.03 | 0.44 (0.51) | 0.03 | 0.48 (0.60) | 0.65 | 0.92 (0.97) |
| | 50 | 0.01 | 0.37 (0.09) | 0.00 | 0.18 (0.06) | 0.14 | 0.66 (0.61) |
| | 60 | $*$ | $*$ (0) | $*$ | $*$ (0) | 0.01 | 0.43 (0.08) |
| 2 | $\leq$ 20 | *1.00* | *1.00* | *1.00* | *1.00* | 1.00 | 1.00 |
| | 30 | 0.97 | *1.00* (0.93) | 0.96 | *1.00* (0.96) | **1.00** | 1.00 |
| | 40 | 0.93 | *1.00* (0.51) | 0.96 | *1.00* (0.60 | **1.00** | *1.00* (0.97) |
| | 50 | 0.92 | 1.00 (0.09) | 0.97 | 1.00 (0.06) | 0.97 | *1.00* (0.61) |
| | 60 | $*$ | $*$ (0) | $*$ | $*$ (0) | 0.96 | 1.00 (0.08) |
| 3 | $\leq$ 20 | | | *1.00* | *1.00* | | |
| | 30 | | | *1.00* | *1.00* (0.96) | | |
| | 40 | | | *1.00* | *1.00* (0.60) | | |
| | 50 | | | 1.00 | 1.00 (0.06) | | |
| | 60 | | | $*$ | $*$ (0) | | |

Table 2: Instantaneous ambiguity success fractions (relative frequencies) for the real data with simulated open-pit using elevation masking (Here, '$\leq \alpha$' refers to the cases with elevation masking less or equal to $\alpha$); For some cases, a fraction of epochs (given in brackets) were processed due to a lack of sufficient visible satellites for positioning (requires at least four satellites)

| Elevation cut-off [deg] | GPS only | | COMPASS only | | GPS + COMPASS | |
|---|---|---|---|---|---|---|
| | Heading | Elevation | Heading | Elevation | Heading | Elevation |
| 10 | 0.02 (0.01) | 0.03 (0.03) | 0.02 (0.02) | 0.04 (0.04) | 0.01 (0.01) | 0.03 (0.02) |
| 20 | 0.02 (0.02) | 0.04 (0.04) | 0.02 (0.02) | 0.04 (0.04) | 0.01 (0.01) | 0.03 (0.03) |
| 30 | 0.02 (0.02) | 0.07 (0.07) | 0.02 (0.02) | 0.05 (0.05) | 0.01 (0.01) | 0.04 (0.04) |
| 40 | 0.03 (0.03) | 0.14 (0.12) | 0.02 (0.02) | 0.07 (0.06) | 0.02 (0.02) | 0.06 (0.06) |
| 50 | $*$ ($*$) | $*$ ($*$) | $*$ ($*$) | $*$ ($*$) | 0.03 (0.03) | 0.17 (0.16) |

Table 3: Empirical and formal (given in brackets) angular standard deviations [deg] for single-frequency data with simulated open-pit using elevation masking

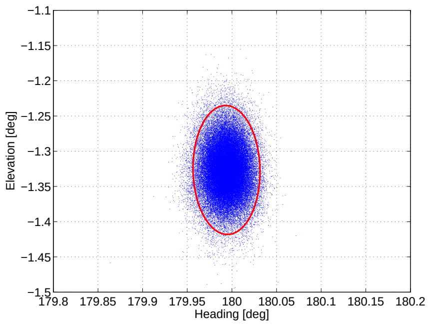


(a) GPS

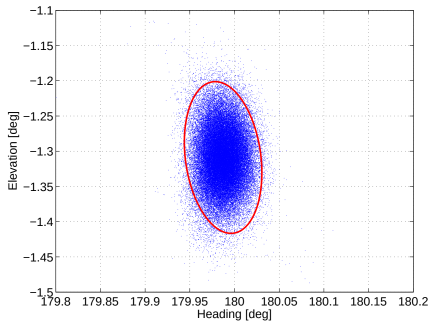


(b) COMPASS

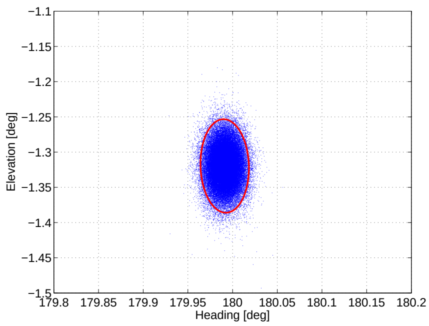


(c) GPS and COMPASS

Figure 4: Scatter plot of the ambiguity fixed attitude angles (the red ellipses correspond to 95% confidence regions)

and C-LAMBDA ambiguity success fractions and ambiguity resolved angular accuracies (standard deviation) for single-, dual-, and triple-frequency processing. The benefits of using C-LAMBDA are highlighted using bold text and the benefits of using multi-frequency processing are highlighted using emphasized text. Using multi-frequency processing, the C-LAMBDA method yields instantaneous attitude determination with as few as six satellites from from GPS and/or COMPASS constellations. The formal standard deviations (terms in brackets) are well in line with the empirical standard deviations confirming the assumed stochastic model parameters in Table 1. A slight degradation of the angular accuracy with the number of satellites can be observed.

### *3.3. Urban Canyon*

In this section the urban canyon impact is analyzed. This is a well-known problem depriving GNSS based navigation solutions in urban environments (Lachapelle et al., 1997; Tsakiri et al., 1998; Ballester-Grpide et al., 2000; Ji et al., 2010). The urban canyon effect has been simulated using a simple model, where we have two buildings as shown in Figure 5 placed symmetrically with respect to the attitude platform on an urban road. The blockage is defined by three angles: $\gamma_0$ the azimuth of the center of the first building (defining the direction of the road), $\alpha_0$ the elevation at the center of the building (defining the height of the buildings), and $\beta_0$ the azimuth angle (defining the width of the buildings). For example, the severity of the blockage (for the case of $\gamma_0 = 90°$, $\alpha_0 = 60°$, and $\beta_0 = 60°$) is shown in Figure 6, which can be compared with the full visibility case of Figure 2. For these parameter values, the model represents two buildings with a height of 9 meters and a width of 17 meters on both sides of a ten-meter wide road in the North-South direction. We considered an urban canyon along a road in North-South direction ($\gamma_0 = 90°$), since this corresponds to the worst case deprivation due to a lack of satellites towards the South direction in Perth, Australia (South polar region).

Table 5 summarize the ambiguity resolution success fraction for single-, dual-, and triple-frequency processing. Note that, for large values of $\alpha_0$ and $\beta_0$, fewer epochs (given in brackets) were processed due to a lack of sufficient visible satellites for positioning (requires at least four satellites). For almost all other cases, instantaneous ambiguity resolution is possible due to the rigorous exploitation of the geometry constraints in the C-LAMBDA method. The corresponding angular accuracies (standard deviations) are reported in Table 6, showing that empirical values are in line with formal values (given in brackets). Both the success fraction and the angular accuracy degrade as the urban canyon effect increases (i.e., angles $\alpha_0$ and $\beta_0$ increase). Except for a few worse case scenarios with large $\alpha_0$ and $\beta_0$, the C-LAMBDA attitude solution using a combined GPS-COMPASS system is available with high ambiguity resolution success fraction as indicated in bold-text in Table 5. The combined system processing not only improves the success fraction but also slightly improves the angular accuracies (Table 6). The ambiguity resolution success fraction and the angular accuracy both degrade, however, as the effect of the urban canyon increases (i.e., angles $\alpha_0$ and $\beta_0$ increase).

| Number of frequency | Number of GPS satellites | Number of COMPASS satellites (PDOP) | Success fraction | | Angular standard deviation [deg] | |
|---|---|---|---|---|---|---|
| | | | LAMBDA | C-LAMBDA | Heading | Elevation |
| 1 | 0 | 4 (9.88) | 0.00 | 0.14 | 0.02 (0.02) | 0.06 (0.06) |
| | | 6 (4.68) | 0.18 | 0.86 | 0.02 (0.02) | 0.05 (0.04) |
| | | 8 (4.03) | 0.49 | 0.97 | 0.02 (0.02) | 0.04 (0.04) |
| | 2 | 4 (6.54) | 0.01 | 0.47 | 0.02 (0.02) | 0.06 (0.06) |
| | | 6 (3.80) | 0.49 | 0.97 | 0.02 (0.02) | 0.04 (0.04) |
| | | 8 (3.36) | 0.77 | 0.99 | 0.02 (0.02) | 0.04 (0.04) |
| | 4 | 0 (7.64) | 0.00 | 0.08 | 0.06 (0.05) | 0.11 (0.10) |
| | | 2 (5.93) | 0.01 | 0.38 | 0.04 (0.04) | 0.07 (0.07) |
| | | 4 (3.28) | 0.42 | 0.95 | 0.02 (0.02) | 0.04 (0.04) |
| | | 6 (2.54) | 0.94 | **1.00** | 0.02 (0.01) | 0.04 (0.03) |
| | | 8 (2.37) | 0.98 | **1.00** | 0.01 (0.01) | 0.03 (0.03) |
| | 6 | 0 (3.23) | 0.10 | 0.76 | 0.02 (0.02) | 0.05 (0.05) |
| | | 2 (2.84) | 0.39 | 0.92 | 0.02 (0.02) | 0.04 (0.04) |
| | | 4 (2.26) | 0.92 | **1.00** | 0.02 (0.01) | 0.04 (0.03) |
| | | $\geq$ 6 (1.90) | 1.00 | 1.00 | 0.01 (0.01) | 0.03 (0.03) |
| | 8 | 0 (2.05) | 0.68 | 0.98 | 0.02 (0.02) | 0.04 (0.04) |
| | | 2 (1.97) | 0.88 | 0.99 | 0.02 (0.01) | 0.03 (0.03) |
| | | 4 (1.81) | 0.99 | **1.00** | 0.01 (0.01) | 0.03 (0.03) |
| | | $\geq$6 (1.63) | 1.00 | 1.00 | 0.01 (0.01) | 0.03 (0.03) |
| | 10 | 0 (1.95) | 0.81 | 0.99 | 0.02 (0.01) | 0.03 (0.03) |
| | | 2 (1.87) | 0.93 | **1.00** | 0.02 (0.01) | 0.03 (0.03) |
| | | 4 (1.73) | 0.99 | **1.00** | 0.01 (0.01) | 0.03 (0.03) |
| | | $\geq$6 (1.57) | 1.00 | 1.00 | 0.01 (0.01) | 0.03 (0.03) |
| 2 | 0 | 4 (9.88) | 0.55 | 0.99 | 0.02 (0.02) | 0.06 (0.05) |
| | | $\geq$6 (4.36) | *1.00* | *1.00* | 0.02 (0.01) | 0.04 (0.04) |
| | 2 | 4 (6.54) | 0.96 | ***1.00*** | 0.03 (0.02) | 0.06 (0.05) |
| | | $\geq$6 (3.58) | *1.00* | *1.00* | 0.02 (0.01) | 0.04 (0.03) |
| | 4 | 0 (7.64) | 0.51 | 0.94 | 0.05 (0.04) | 0.09 (0.08) |
| | | 2 (5.93) | 0.93 | ***1.00*** | 0.03 (0.03) | 0.06 (0.05) |
| | | $\geq$4 (2.73) | *1.00* | *1.00* | 0.01 (0.01) | 0.03 (0.03) |
| | 6 | 0 (3.23) | 0.97 | ***1.00*** | 0.02 (0.02) | 0.04 (0.04) |
| | | $\geq$2 (2.21) | *1.00* | *1.00* | 0.01 (0.01) | 0.03 (0.03) |
| | $\geq$ 8 | $\geq$ 0 (1.76) | *1.00* | *1.00* | 0.01 (0.01) | 0.03 (0.03) |
| 3 | 0 | 4 (9.88) | *1.00* | *1.00* | 0.02 (0.02) | 0.06 (0.04) |
| | | $\geq$6 (4.35) | 1.00 | 1.00 | 0.02 (0.01) | 0.04 (0.03) |

Table 4: Instantaneous ambiguity success fractions (relative frequencies), and empirical and formal (given in brackets) angular standard deviations (based on correctly fixed epochs) for the experiment with simulated satellite outage (Here, '$\geq s$' refers to $s$ or more satellites)

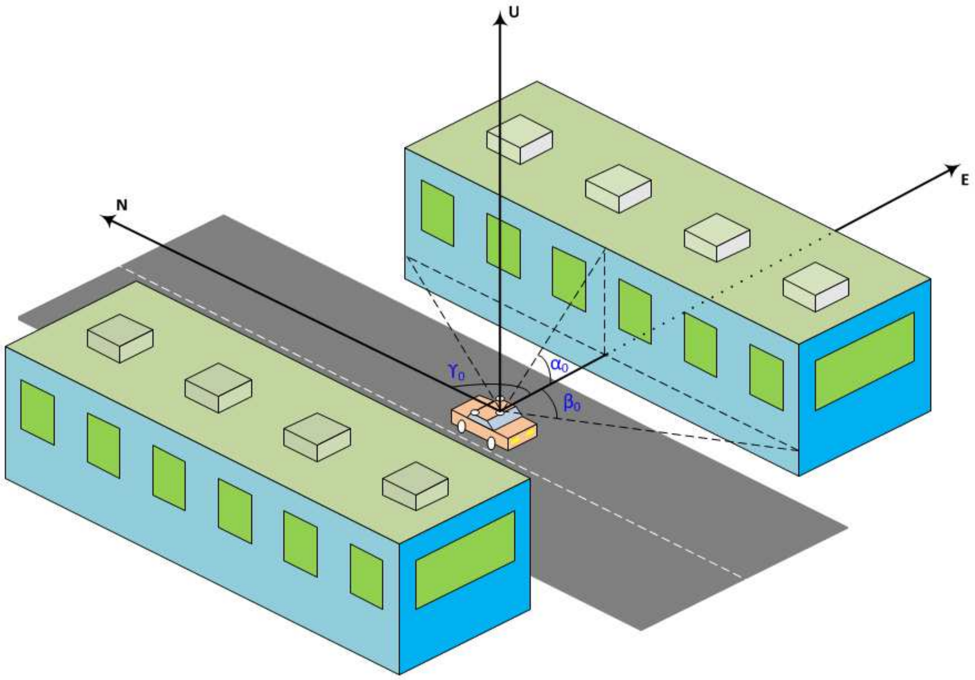


Figure 5: Simulated urban canyon: Buildings on both sides of an urban road block satellite visibility; Angle $\gamma_0$ defines the direction of the road, while angles $\alpha_0$ and $\beta_0$ define the height and the width of the buildings, respectively.

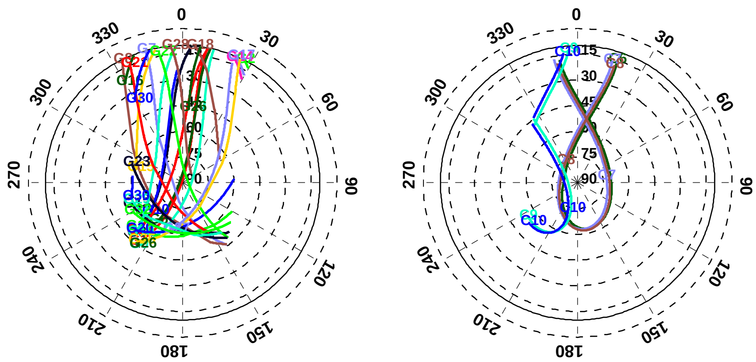

(a) Skyplot (GPS) (b) Skyplot (COMPASS)

Figure 6: Satellite visibility for simulated urban canyon with $\alpha_0 = 60°$ and $\beta_0 = 60°$ in the North-South direction

| Number of frequency | $\alpha_0$ [deg] | $\beta_0$ [deg] | GPS only | | COMPASS only | | GPS + COMPASS | |
|---|---|---|---|---|---|---|---|---|
| | | | LAMBDA | C-LAMBDA | LAMBDA | C-LAMBDA | LAMBDA | C-LAMBDA |
| 1 | 20 | 20 | 0.77 | 0.98 | 0.51 | 0.97 | **1.00** | **1.00** |
| | | 40 | 0.72 | 0.98 | 0.50 | 0.96 | **1.00** | **1.00** |
| | | 60 | 0.68 | 0.97 | 0.50 | 0.96 | **1.00** | **1.00** |
| | | 80 | 0.68 | 0.97 | 0.50 | 0.96 | **1.00** | **1.00** |
| | 40 | 20 | 0.64 | 0.96 | 0.42 | 0.94 (0.99) | **1.00** | **1.00** |
| | | 40 | 0.42 | 0.89 (0.98) | 0.21 | 0.81 (0.97) | **1.00** | **1.00** |
| | | 60 | 0.21 | 0.77 (0.93) | 0.21 | 0.80 (0.96) | 0.98 | **1.00** |
| | | 80 | 0.17 | 0.75 (0.91) | 0.21 | 0.80 (0.96) | 0.98 | **1.00** |
| | 60 | 20 | 0.52 | 0.92 | 0.35 | 0.90 (0.99) | **1.00** | **1.00** |
| | | 40 | 0.20 | 0.68 (0.95) | 0.11 | 0.58 (0.87) | 0.92 | **1.00** |
| | | 60 | 0.02 | 0.35 (0.57) | 0.01 | 0.30 (0.27) | 0.34 | 0.78 (0.92) |
| | | 80 | 0.02 | 0.32 (0.34) | 0.00 | 0.14 (0.09) | 0.20 | 0.66 (0.75) |
| | 80 | 20 | 0.43 | 0.86 | 0.27 | 0.83 (0.98) | 0.99 | **1.00** |
| | | 40 | 0.10 | 0.51 (0.88) | 0.05 | 0.41 (0.73) | 0.74 | 0.97 |
| | | 60 | 0.00 | 0.14 (0.13) | 0.00 | 0.08 (0.03) | 0.04 | 0.38 (0.47) |
| | | 80 | ∗ | ∗ (0) | ∗ | ∗ (0) | 0.00 | 0.14 (0.04) |
| 2 | 20 | ≤80 | *1.00* | *1.00* | *1.00* | *1.00* | 1.00 | 1.00 |
| | 40 | 20 | *1.00* | *1.00* | *1.00* | *1.00* (0.99) | 1.00 | 1.00 |
| | | 40 | 0.99 | *1.00* (0.98) | 0.98 | *1.00* (0.97) | **1.00** | **1.00** |
| | | 60 | 0.98 | *1.00* (0.93) | 0.98 | *1.00* (0.96) | ***1.00*** | **1.00** |
| | | 80 | 0.97 | *1.00* (0.91) | 0.98 | *1.00* (0.96) | ***1.00*** | **1.00** |
| | 60 | 20 | 0.99 | *1.00* | 0.99 | *1.00* (0.99) | **1.00** | 1.00 |
| | | 40 | 0.94 | *1.00* (0.95) | 0.93 | *1.00* (0.87) | **1.00** | **1.00** |
| | | 60 | 0.80 | 0.99 (0.57) | 0.79 | *1.00* (0.27) | 0.97 | *1.00* (0.92) |
| | | 80 | 0.82 | 0.98 (0.34) | 0.81 | *1.00* (0.09) | 0.94 | *1.00* (0.75) |
| | 80 | 20 | 0.98 | *1.00* | 0.98 | *1.00* (0.98) | **1.00** | 1.00 |
| | | 40 | 0.89 | 0.99 (0.88) | 0.79 | 0.99 (0.73) | ***1.00*** | **1.00** |
| | | 60 | 0.58 | 0.96 (0.13) | 0.70 | 0.99 (0.03) | 0.78 | 0.98 (0.47) |
| | | 80 | ∗ | ∗ (0) | ∗ | ∗ (0) | 0.69 | 0.97 (0.04) |
| 3 | 20 | ≤80 | | | *1.00* | *1.00* | | |
| | 40 | ≤80 | | | *1.00* | *1.00* (0.97) | | |
| | 60 | 20 | | | *1.00* | *1.00* (0.99) | | |
| | | 40 | | | *1.00* | *1.00* (0.87) | | |
| | | 60 | | | *1.00* | *1.00* (0.27) | | |
| | 80 | 20 | | | *1.00* | *1.00* (0.98) | | |
| | | 40 | | | *1.00* | *1.00* (0.73) | | |

Table 5: Instantaneous ambiguity success fractions (relative frequencies) for the experiment with simulated urban canyon (Figure 5); Here, '$\leq\ \alpha$' refers to less or equal to $\alpha$; For some cases, a fraction of epochs (given in brackets) were processed due to not enough satellites for positioning (requires at least four satellites)

| $\alpha_0$ [deg] | $\beta_0$ [deg] | GPS only | | COMPASS only | | GPS + COMPASS | |
|---|---|---|---|---|---|---|---|
| | | Heading | Elevation | Heading | Elevation | Heading | Elevation |
| 20 | 20 | 0.02 (0.01) | 0.04 (0.04) | 0.02 (0.02) | 0.04 (0.04) | 0.01 (0.01) | 0.03 (0.03) |
| | 40 | 0.02 (0.01) | 0.04 (0.04) | 0.02 (0.02) | 0.04 (0.04) | 0.01 (0.01) | 0.03 (0.03) |
| | 60 | 0.02 (0.01) | 0.04 (0.04) | 0.02 (0.02) | 0.04 (0.04) | 0.01 (0.01) | 0.03 (0.03) |
| | 80 | 0.02 (0.01) | 0.04 (0.04) | 0.02 (0.02) | 0.04 (0.04) | 0.01 (0.01) | 0.03 (0.03) |
| 40 | 20 | 0.02 (0.02) | 0.04 (0.04) | 0.02 (0.02) | 0.04 (0.04) | 0.01 (0.01) | 0.03 (0.03) |
| | 40 | 0.02 (0.02) | 0.05 (0.05) | 0.02 (0.02) | 0.05 (0.05) | 0.01 (0.01) | 0.03 (0.03) |
| | 60 | 0.02 (0.02) | 0.08 (0.06) | 0.02 (0.02) | 0.05 (0.05) | 0.01 (0.01) | 0.04 (0.03) |
| | 80 | 0.02 (0.02) | 0.08 (0.07) | 0.02 (0.02) | 0.05 (0.05) | 0.01 (0.01) | 0.04 (0.03) |
| 60 | 20 | 0.02 (0.02) | 0.04 (0.04) | 0.02 (0.02) | 0.04 (0.04) | 0.01 (0.01) | 0.03 (0.03) |
| | 40 | 0.02 (0.02) | 0.05 (0.05) | 0.02 (0.02) | 0.05 (0.05) | 0.02 (0.02) | 0.04 (0.03) |
| | 60 | 0.04 (0.04) | 0.06 (0.06) | 0.03 (0.02) | 0.05 (0.05) | 0.03 (0.03) | 0.05 (0.05) |
| | 80 | 0.04 (0.04) | 0.07 (0.07) | $*$ ($*$) | $*$ ($*$) | 0.03 (0.03) | 0.07 (0.07) |
| 80 | 20 | 0.02 (0.02) | 0.04 (0.04) | 0.02 (0.02) | 0.04 (0.04) | 0.01 (0.01) | 0.03 (0.03) |
| | 40 | 0.03 (0.03) | 0.05 (0.05) | 0.02 (0.02) | 0.05 (0.05) | 0.02 (0.02) | 0.04 (0.04) |
| | 60 | $*$ ($*$) | $*$ ($*$) | $*$ ($*$) | $*$ ($*$) | 0.06 (0.05) | 0.04 (0.04) |

Table 6: Empirical and formal (given in brackets) angular standard deviations [deg] for single-frequency data with simulated urban canyon (Figure 5)

## 4. Conclusions

In this contribution we studied the use of the combined GPS-COMPASS constellation for C-LAMBDA attitude determination. In comparing the performances of LAMBDA and C-LAMBDA, we also studied the impact of using the known baseline length on ambiguity resolution. Using data from a real data campaign spanning 23 days, improved availability and angular accuracy were demonstrated using single epoch GPS/COMPASS processing. We considered various satellite deprived environments (satellite outages, urban canyon, and open-pit) to study the robustness of the GPS/COMPASS-based attitude solutions. Using simulated satellite outages, we showed that instantaneous multi-frequency ambiguity resolution using the C-LAMBDA method is possible with as few as six satellites from GPS and/or COMPASS constellations. We also showed that the use of a combined constellation significantly improves the attitude solution availability in an urban canyon. Finally, we showed that the use of the combined constellation yields instantaneous attitude solutions in an open-pit with as large as 30 degree elevation masking even with single frequency precessing, while one can go up to only 20 degree elevation masking with multi-frequency processing of an individual system. Important for future research in the field of GNSS attitude determination is the further development of a probabilistic framework, similar to the one already available for the standard mixed-integer GNSS model (Teunissen, 2002; Verhagen and Teunissen, 2006b). Such theoretical framework would allow for the development of the appropriate probability density functions and test statistics for the constrained GNSS attitude model.

## Acknowledgement

The second author P. J. G. Teunissen is the recipient of an Australian Research Council Federation Fellowship (project number FF0883188). Post-processed orbit and clock products were kindly provided by Peter Steigenberger from Technische Universität München, Germany. All these supports are gratefully acknowledged.

## References

Ballester-Grpide, I., Herriz-Monseco, E., andMiguel M. Romay-Merino, A. J.-M., Beech, T. W., September 2000. Future GNSS constellation performances inside urban environments. In: Proceedings of the 13th International Technical Meeting of the Satellite Division of The Institute of Navigation (ION GPS 2000). Salt Lake City, UT, pp. 2436–2445.

Boon, F., Ambrosius, B., 1997. Results of real-time applications of the LAMBDA method in GPS based aircraft landings. In: Proceedings KIS97. pp. 339–345.

Buist, P. J., 2007. The baseline constrained LAMBDA method for single epoch, single frequency attitude determination applications. In: Proceedings of the 20th International Technical Meeting of the Satellite Division of The Institute of Navigation (ION GNSS 2007). Fort Worth, TX, USA, pp. 2962 – 2973.

Cao, C., Jing, G., Luo, M., 56 Novmber 2008. COMPASS satellite navigation system development. In: PNT challenges and opportunities symposium. Stanford, California, USA.

Chen, H., Huang, Y., Chiang, K., Yang, M., Rau, R., 2009. The performance comparison between GPs and BeiDou-2/compass: A perspective from Asia. Journal of the Chinese institute of engineers 32 (5), 679–689.

Cohen, C., 1992. Attitude determination using GPS. Ph.D. thesis, Stanford University.

Cox, D., 1999. Integration of LAMBDA ambiguity resolution with Kalman filter for relative navigation of spacecraft. In: Institute of Navigation, Annual Meeting, 55 th, Cambridge, MA. pp. 739–745.

Crassidis, J. L., Markley, F. L., 1997. New algorithm for attitude determination using Global Positioning System signals. Journal of Guidance, Control, and Dynamics 20 (5), 891–896.

CSNO, December 2011. BeiDou navigation satellite system signal in space interface control document: Open Service Signal B1I. Tech. rep., China Satellite Navigation Office, version 1.0.

Euler, H.-J., Goad, C., 1991. On optimal filtering of GPS dual frequency observations without using orbit information. Journal of Geodesy 65, 130–143.

Giorgi, G., Buist, P., 2008. Single-epoch, single-frequency, standalone full attitude determination: experimental results. In: Proceedings of the 4th ESA Workshop on Satellite Navigation User Equipment Technologies, NAVITEC. ESA-ESTEC, The Netherlands, p. 8.

Giorgi, G., Teunissen, P. J. G., Buist, P. J., 2008. A search and shrink approach for the baseline constrained LAMBDA method: Experimental results. In: Yasuda, A. (Ed.), Proceedings of International Symposium on GPS/GNSS. Tokyo University of Marine Science and Technology, pp. 797 – 806.

Giorgi, G., Teunissen, P. J. G., Gourlay, T. P., July 2012a. Instantaneous Global Navigation Satellite System (GNSS)-based attitude determination for maritime applications. Oceanic Engineering, IEEE Journal of 37 (3), 348 –362.

Giorgi, G., Teunissen, P. J. G., Verhagen, S., Buist, P. J., 2010. Testing a new multivariate GNSS carrier phase attitude determination method for remote sensing platforms. Advances in Space Research 46 (2), 118 – 129.

Giorgi, G., Teunissen, P. J. G., Verhagen, S., Buist, P. J., 2012b. Instantaneous ambiguity resolution in Global-Navigation-Satellite-System-based attitude determination applications: A multivariate constrained approach. Journal of Guidance, Control, and Dynamics 35 (1), 51–67.

Grelier, T., Ghion, A., Dantepal, J., Ries, L., DeLatour, A., Issler, J.-L., Avila-Rodriguez, J., Wallner, S., GW, H., September 2007. Compass signal structure and first measurements. In: Proceedings of ION GNSS-2007. Fort Worth, TX, p. 30153024.

Harville, D. A., 1997. Matrix Algebra From A Statisticians Perspective. Springer, New York.

Huang, S., Wang, J., Wang, X., Chen, J., 2009. The application of the LAMBDA method in the estimation of the GPS slant wet vapour. Acta Astronomica Sinica 50, 60–68.

Ji, S., Chen, W., Ding, X., Chen, Y., Zhao, C., Hu, C., 2010. Potential benefits of GPS/GLONASS/Galileo integration in an urban canyon - Hong Kong. The Journal of Navigation 63 (04), 681–693.

Ji, S., Chen, W., Zhao, C., Ding, X., Chen, Y., 2007. Single epoch ambiguity resolution for Galileo with the CAR and LAMBDA methods. GPS Solutions 11, 259–268.

Jin, S., Luo, O., Ren, C., 2010. Effects of physical correlations on long-distance gps positioning and zenith tropospheric delay estimates. Advances in Space Research 46 (2), 190–195.

Jin, S., Wang, J., Park, P.-H., 2005. An improvement of gps height estimations-stochastic modeling. Earth, Planets, and Space 57 (4), 253–259.

Kroes, R., Montenbruck, O., Bertiger, W., Visser, P., 2005. Precise GRACE baseline determination using GPS. GPS Solutions 9, 21–31.

Lachapelle, G., Ryan, S., Petovello, M., Stephen, J., 1997. Augmentation of GPS/GLONASS for vehicular navigation under signal masking. In: Proceedings of the 10th International Technical Meeting of the Satellite Division of The Institute of Navigation (ION GPS 1997). pp. 1511–1519.

Li, Y., Zhang, K., Roberts, C., Murata, M., 2004. On-the-fly GPS-based attitude determination using single- and double-differenced carrier phase measurements. GPS Solutions 8 (2), 93–102.

Lin, D., Voon, L., Nagarajan, N., 2004. Real-time attitude determination for microsatellite by LAMBDA method combined with Kalman filtering. In: 22 nd AIAA International Communications Satellite Systems Conference and Exhibit 2004. Monterey, California, USA.

Lu, G., 1995. Development of a GPS multi-antenna system for attitude determination. Ph.D. thesis, Department of Geomatics Engineering, University of Calgary.

Madsen, J., Lightsey, E. G., July-August 2004. Robust spacecraft attitude determination using global positioning system receivers. Journal of Spacecraft and Rockets 41 (4), 635–643.

Magnus, J. R., Neudecker, H., 1995. Matrix differential calculus with applications in statistics and econometrics. Wiley, New York.

Montenbruck, O., Hauschild, A., Steigenberger, P., Hugentobler, U., Riley, S., 23-27 July 2012a. A COMPASS for Asia: First Experience with the BeiDou-2 Regional Navigation System. In: IGS Workshop. Olsztyn, Poland.

Montenbruck, O., Hauschild, A., Steigenberger, P., Hugentobler, U., Teunissen, P. J. G., Nakamura, S., 2012b. Initial assessment of the COMPASS/BeiDou-2 regional navigation satellite system. GPS Solutions.

Park, C., Teunissen, P. J. G., 2003. A new carrier phase ambiguity estimation for GNSS attitude determination systems. In: Proceedings of International Symposium on GPS/GNSS. Tokyo, Japan, pp. 283–290.

Park, C., Teunissen, P. J. G., 2009. Integer least squares with quadratic equality constraints and its application to GNSS attitude determination systems. International Journal of Control, Automation, and Systems 7 (4), 566–576.

Park, S.-Y., 2002. Thermally induced attitude disturbance control for spacecraft with a flexible boom. Journal of Spacecraft and Rockets 39, 325–328.

Psiaki, M. L., September-October 2006. Batch algorithm for global-positioning-system attitude determination and integer ambiguity resolution. Journal od Guidance, Control, and Dynamics 29 (5), 1070–1079.

Shi, C., Zhao, Q., Li, M., Tang, W., Hu, Z., Lou, Y., Zhang, H., Niu, X., Liu, J., 2012. Precise orbit determination of Beidou Satellites with precise positioning. Science China Earth Sciences 55, 1079–1086.

Steigenberger, P., Hauschild, A., Montenbruck, O., Hugentobler, U., 23-27 July 2012a. Performance analysis of COMPASS orbit and clock determination and COMPASS-only PPP. In: IGS Workshop. Olsztyn, Poland.

Steigenberger, P., Hauschild, A., Montenbruck, O., Rodriguez-Solano, C., Hugentobler, U., 2012b. Orbit and clock determination of QZS-1 based on the CONGO network. In: ION-ITM-2012. Newport Beach, California.

Teunissen, P. J. G., 1995. The least-squares ambiguity decorrelation adjustment: a method for fast GPS integer ambiguity estimation. Journal of Geodesy 70, 65–82.

Teunissen, P. J. G., 1999. An optimality property of the integer least-squares estimator. Journal of Geodesy 73, 587–593.

Teunissen, P. J. G., 2002. The parameter distributions of the integer GPS model. Journal of Geodesy 76 (1), 41–49.

Teunissen, P. J. G., 2006. The LAMBDA method for the GNSS compass. Artificial Satellites 41 (3), 89–103.

Teunissen, P. J. G., 2010. Integer least-squares theory for the GNSS compass. Journal of Geodesy 84 (7), 433–447.

Teunissen, P. J. G., De Jonge, P., Tiberius, C., 1997. Performance of the LAMBDA method for fast GPS ambiguity resolution. Navigation 44 (3), 373–383.

Teunissen, P. J. G., Giorgi, G., Buist, P. J., 2011. Testing of a new single-frequency GNSS carrier phase attitude determination method: Land, ship and aircraft experiments. GPS Solutions 15 (1), 15–28.

Teunissen, P. J. G., Kleusberg, A., 1998. GPS for Geodesy, 2nd Edition. Springer.

Tsakiri, M., Stewart, M., Forward, T., Sandison, D., Walker, J., 1998. Urban fleet monitoring with GPS and GLONASS. The Journal of Navigation 51 (03), 382–393.

Verhagen, S., Joosten, P., 2003. Algorithms for design computations for integrated GPS-Galileo. In: Proceedings of the European Navigation Conference (ENC-GNSS 2003).

Verhagen, S., Teunissen, P. J. G., 2006a. New global navigation satellite system ambiguity resolution method compared to existing approaches. Journal of Guidance, Control, and Dynamics 29 (4), 981–991.

Verhagen, S., Teunissen, P. J. G., 2006b. On the probability density function of the ambiguity residuals. GPS Solutions 10 (1), 21–28.

Yang, Y., Li, J., Xu, J., Tang, J., Guo, H., He, H., 2011. Contribution of the Compass satellite navigation system to global PNT users. Chinese Science Bulletin 56 (26), 2813–2819.

Zhang, S., Guo, J., Li, B., Rizos, C., 1820 August 2011. An analysis of satellite visibility and relative positioning precision of COMPASS. In: Proceedings of Symposium for Chinese professionals in GPS. Shanghai, Peoples Republic of China, pp. 41–46.